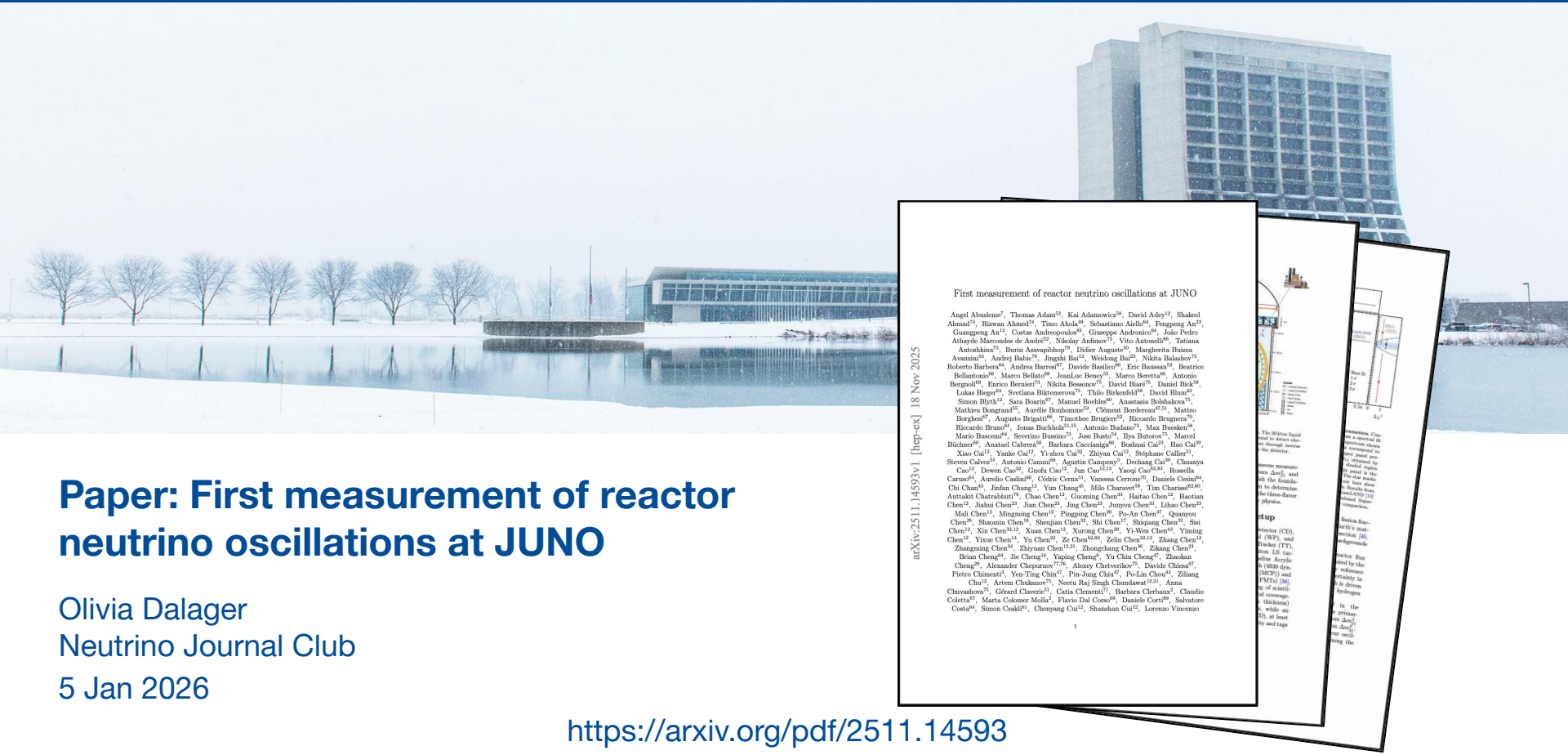

Paper: First measurement of reactor neutrino oscillations at JUNO

Olivia Dalager

Neutrino Journal Club

5 Jan 2026

https://arxiv.org/pdf/2511.14593

Outline

1. Introduction & Motivation *(pages 9-10, 16)*
2. Experimental Design *(pages 10-11, 16-18)*
3. Calibration & Reconstruction *(pages 11-12, 18-20)*
4. Analysis *(page 15)*
    a. Selection *(pages 12-14, 20-25)*
    b. Background Evaluation *(pages 13, 22-24)*
    c. Reactor-Neutrino Signal Prediction *(pages 13-14, 24-25)*
5. Spectral Fit & Results *(pages 14-15, 25-26)*
6. Discussion & Outlook *(page 15)*

Introduction & Motivation

- JUNO was proposed to determine the neutrino mass ordering
- Detects electron antineutrinos produced by β-decays in nuclear reactors

Fig. 5 Reactor neutrino oscillation at different baselines. Survival probability $\mathcal{P}_{ee}$ of 4 MeV reactor $\bar{\nu}_e$ vs. baseline. Red: slow solar oscillation (Δm^2_{21}); blue: total $\mathcal{P}ee$ including fast atmospheric oscillations (Δm^2_{31}). Experimental baselines: JUNO (orange, 52.5 km) near solar oscillation maximum, Daya Bay near/far (pink), KamLAND (green). Circle sizes scale with detector sizes.

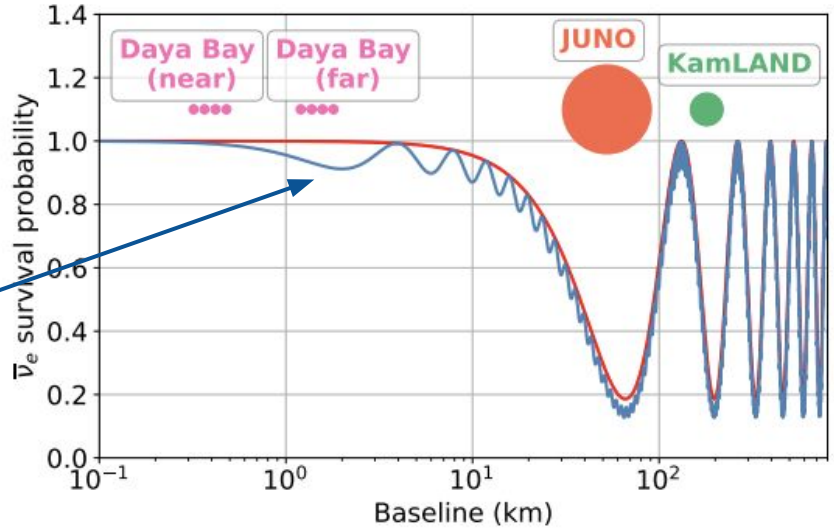

$$\mathcal{P}_{ee} = 1 - \sin^2 2\widetilde{\theta}_{12}\, \tilde{c}^4_{13}\, \sin^2 \widetilde{\Delta}_{21} - \sin^2 2\widetilde{\theta}_{13} \left(\tilde{c}^2_{12} \sin^2 \widetilde{\Delta}_{31} + \tilde{s}^2_{12} \sin^2 \widetilde{\Delta}_{32} \right), \quad (1)$$

Fermilab

Experimental Design

- **650 m of rock overburden** (~1800 m water equivalent)
- **20 kton of liquid scintillator** in the Central Detector
- 17,596 20-inch (large) PMTs
- 25,587 3-inch (small) PMTs
- **Outer Water Cherenkov Detector** for shielding against radioactivity and tagging cosmic muons
- **Top Tracker** provides high-purity and high-precision muon sample

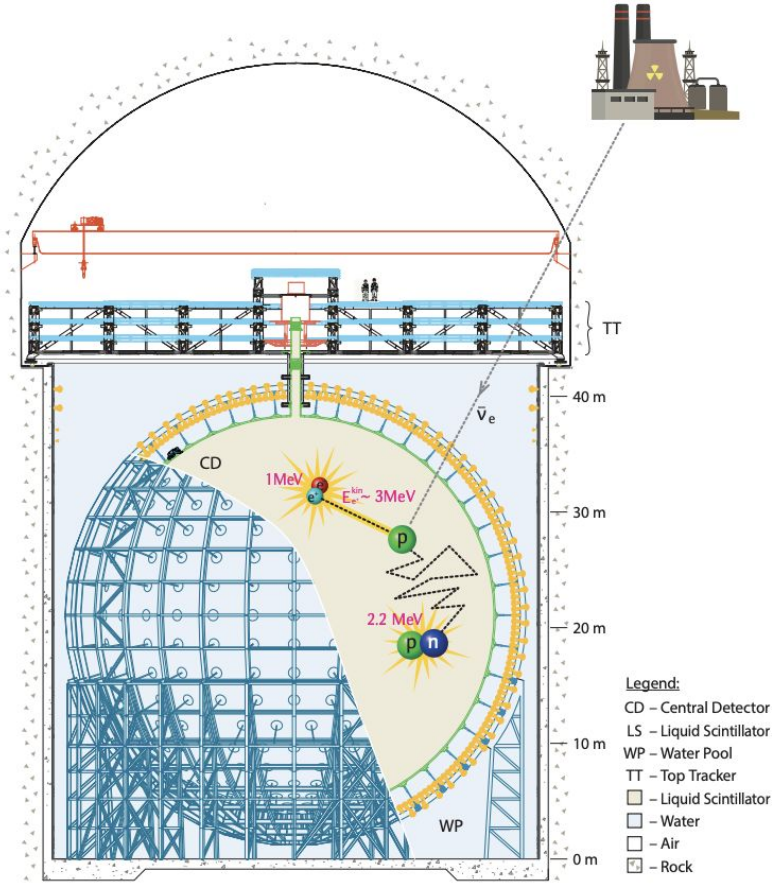

Fig. 1 JUNO experimental layout. The 20 kton liquid scintillator detector is located underground to detect electron antineutrinos from nuclear reactors through inverse beta decay interaction, cartooned inside the detector.

Fermilab

Calibration & Reconstruction

- Detector response calibrated via radioactive sources and naturally occurring backgrounds
  1. Light yield
  2. Event reconstruction
  3. **Energy resolution**
  4. Non-linearity of the energy scale
  5. Residual spatial non-uniformity

Fig. 2 JUNO energy scale uncertainty. a, Reconstructed energy E_{rec} of the neutron-capture peak (E_γ = 2.223 MeV, dashed line) from AmC neutron sources and antineutrino candidates across the full detector volume. The gray markers indicate neutrons outside the fiducial volume (FV). **b**, Residual energy bias and systematic uncertainty for γ sources at fixed calibration positions, α-decays from natural radioactivity, and neutrons from muon-induced spallation and antineutrino candidates. $\langle E \rangle$ refers to expected reconstructed energy of each source at the center. Error bars includes residual temporal- and spatial-variations, and the band represents the estimated overall systematic uncertainty of the energy scale.

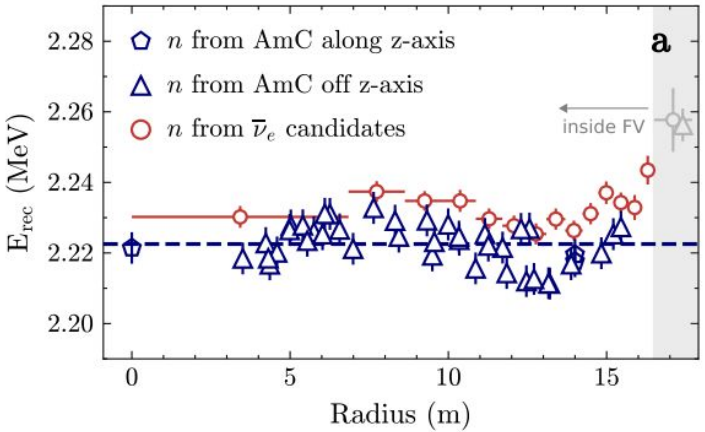

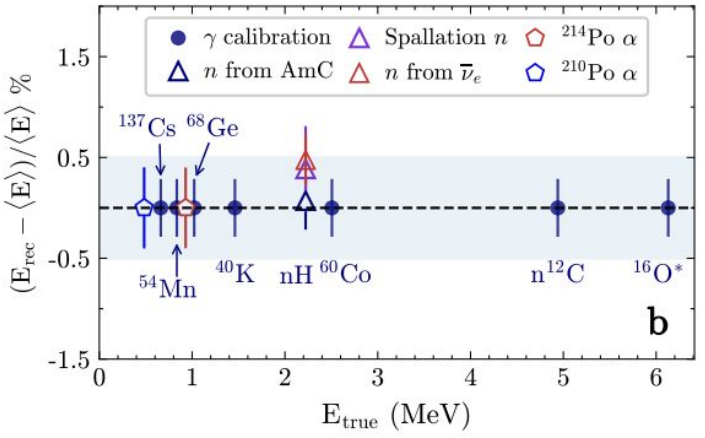

Fermilab

Calibration & Reconstruction

- Detector response calibrated via radioactive sources and naturally occurring backgrounds
  1. Light yield
  2. Event reconstruction
  3. Energy resolution
  4. **Non-linearity of the energy scale**
  5. Residual spatial non-uniformity

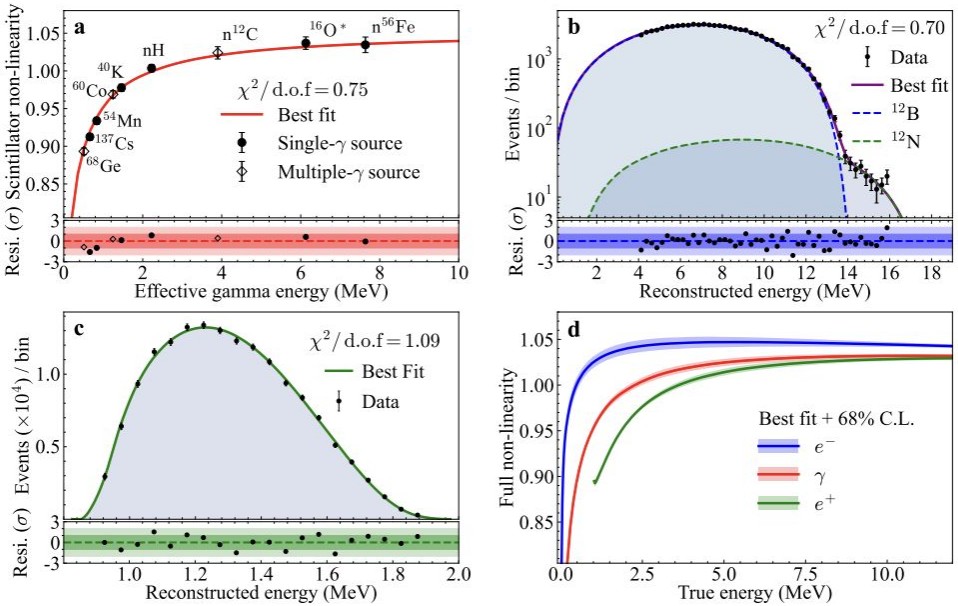

Fig. 6 Energy scale non-linearity calibration. a, Scintillator non-linearity from γ calibration sources deployed at the detector's center: single-γ sources (solid circle), multi-γ sources (hollow rhombus), and the best-fit curve (red). **b**, Measured cosmogenic ^{12}B β^- spectrum (points) compared to prediction (blue line), with a best-fit ^{12}N component (green dashed line)of 2.7% identified via its high-energy shoulder. **c**, Measured ^{11}C β^+ spectrum (points) and the best-fit model (green line). **d**, Non-linearity response model for electrons (blue), γ's (red), and positrons (green).

Data Analysis: Selection (1)

- 3 independent analyses
- 59.1 days of data (across 69 days)
- Inverse Beta Decays (IBDs) interactions:

$$\overline{\nu}_e + p \rightarrow e^+ + n$$

  - Prompt signal: positron annihilation
    - $E_p \approx E_{\overline{\nu}_e} - 0.784\ \mathrm{MeV}$
  - Delayed signal: neutron capture
    - τ ~ 200 μs

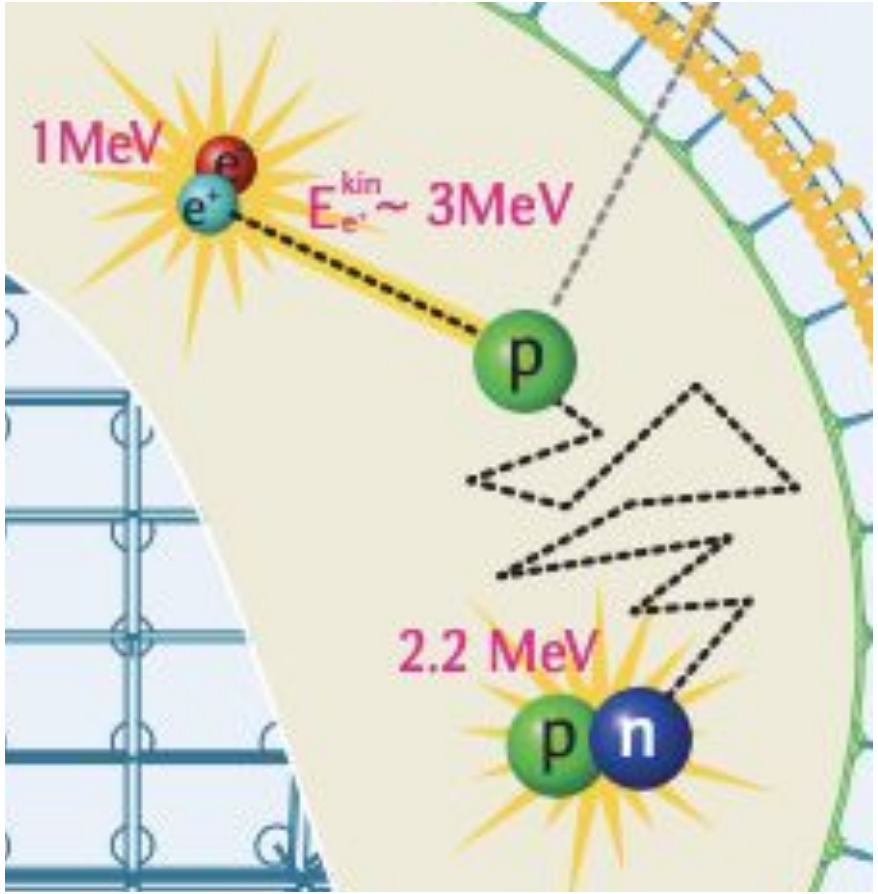

Fermilab

Data Analysis: Selection (2)

- Spatio-temporal coincidence
  - **Prompt energy cut:** 0.7 MeV < E_p < 12 MeV
  - **Delayed energy cut:** 2.0 MeV < E_d < 2.5 MeV
  - **Time interval**: 5 μs < Δt < 1 ms
  - **Spatial separation:** Δd < 1.5 m
- Fiducial volume cuts
  - r < 16.5 m, |z| < 15.5 m
- Muon veto
  - Temporal veto applied to remove short-lived backgrounds
  - Spatio-temporal veto around spallation neutrons to suppress long-lived backgrounds
- Multiplicity cut
  - Reduce instrumental + multiple particle coincidence backgrounds

Antineutrinos ($\bar{\nu}_e$) Candidates Summary		
DAQ live time (days)	59.1	
$\bar{\nu}_e$ candidates	2379	
Selection Efficiencies (%)	ε	σ_{rel}
Fiducial volume	80.6	1.6
PMT flasher rejection	>99.9	negligible
μ veto	93.6	negligible
Multiplicity	97.4	negligible
Prompt-delayed coinc.	95.1	0.13
Total efficiency ($\varepsilon_{\mathrm{tot}}$)	69.9	1.6
$\bar{\nu}_e$ signal (cpd[1])		
w/o $\varepsilon_{\mathrm{tot}}$ corrected	33.5 ± 1.7	
w/ $\varepsilon_{\mathrm{tot}}$ corrected	47.9 ± 2.6	
Non-oscillated $\bar{\nu}_e$	150.9 ± 2.7	

Table 1 Event selection and backgrounds. The table lists the IBD selection criteria with their respective efficiencies (ε) and relative uncertainties (σ_{rel}), alongside the measured or expected pre-fit and best-fit background rates. The $\bar{\nu}_e$ signal rates were derived both with and without applying the efficiency correction to the observed IBD rate, after background subtraction. The non-oscillated prediction is based on reactor operational data and the flux model described in Methods. The best-fit values for the backgrounds come from the spectral fit.

[1]cpd ≡ counts per day

Reactor Neutrino Candidate Characteristics (1)

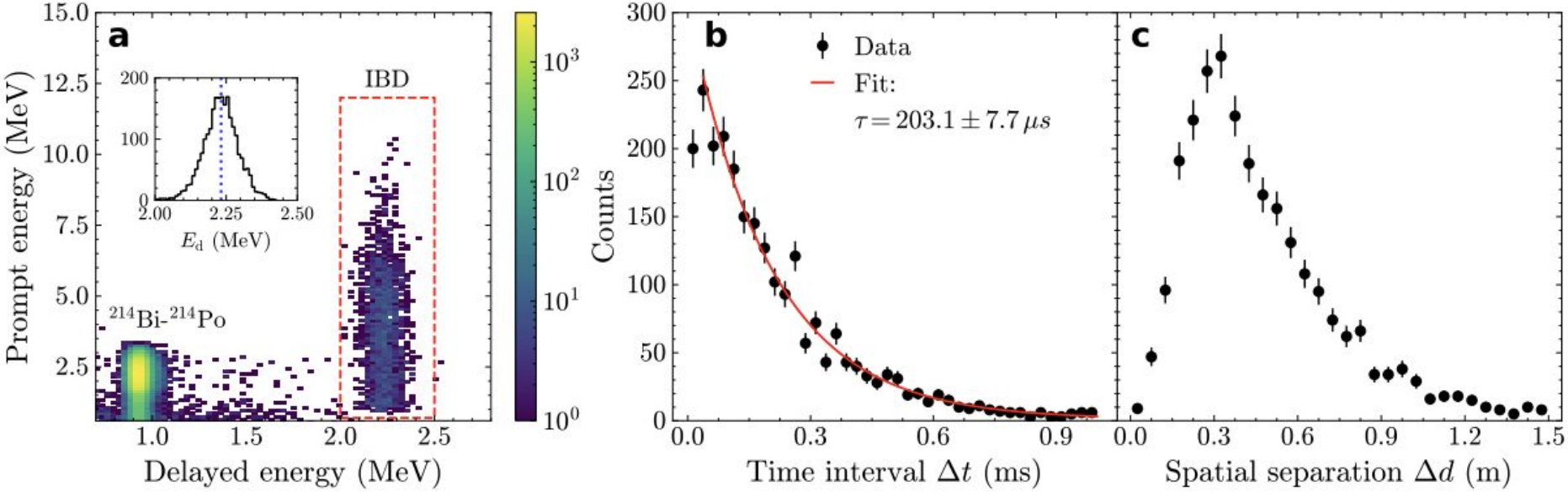

Fig. 7 Reactor neutrino candidates characteristics. a, Two-dimensional prompt-versus-delayed energies (with enlarged delayed energy window) showing the ^{214}Bi-^{214}Po cluster at $E_d \sim 1$ MeV and the IBD selection region (dashed red box). The inset shows the delayed-energy spectrum, featuring a clear neutron-capture peak at $E_d \simeq 2.23$ MeV (blue dashed line). **b,** Temporal correlation following an exponential decay with a fitted neutron-capture time of $\tau = 203.1 \pm 7.7$ μs. The deviation of the first point is due to the $\Delta t > 5$ μs cut and is therefore not included in the fit. **c,** Spatial separation Δd of the prompt and delayed vertices.

Reactor Neutrino Candidate Characteristics (2)

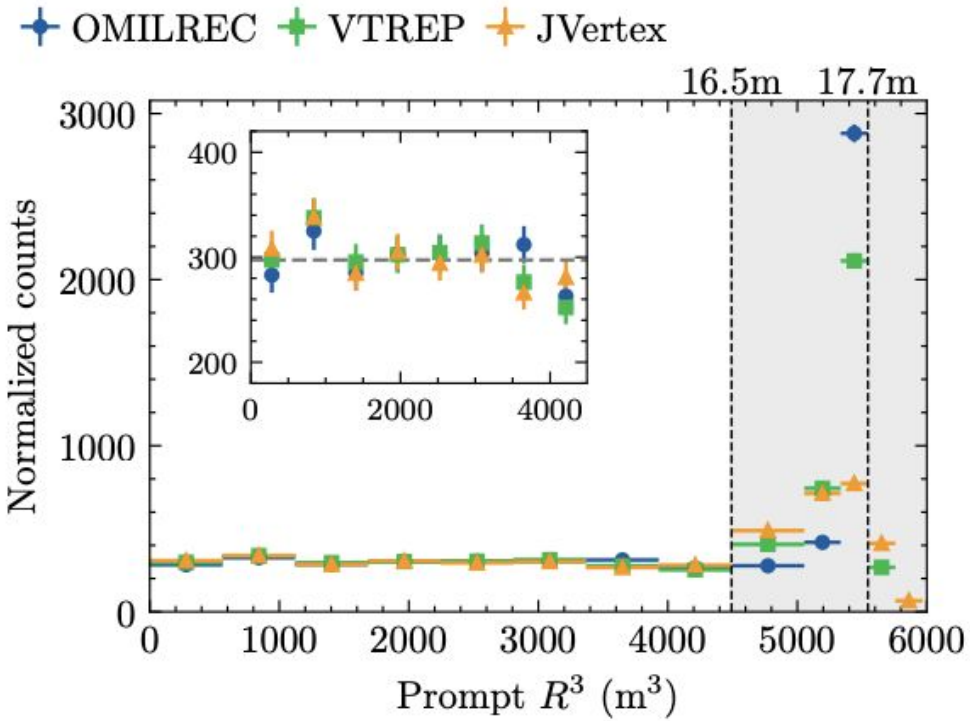

Fig. 8 Spatial distribution of reactor neutrino candidates. Prompt-event counts versus reconstructed cubic radius (R^3) are shown for the three vertex algorithms: OMILREC (blue), VTREP (green), and JVertex (orange). Horizontal bars indicate R^3 bin widths; vertical dashed lines mark the FV boundary (16.5 m) and detector edge (17.7 m). The inset shows the uniform event density within the FV, with the dashed line indicating the mean count level. The rising counts beyond the FV are primarily due to accidental coincidences, with minor contributions from fast- and double-neutron backgrounds.

Fermilab

Data Analysis: Background Evaluation (1)

- Main backgrounds:
  1. Cosmogenic ^{9}Li/^{8}He
  2. Geoneutrinos
  3. Antineutrinos from other reactors around the world
  4. ^{214}Bi-^{214}Po

Backgrounds (cpd)	Pre-fit	Best-fit
^{9}Li/^{8}He	4.3 ± 1.4	3.9 ± 0.6
Geoneutrinos	1.2 ± 0.5	1.4 ± 0.4
World reactors	0.88 ± 0.09	0.88 ± 0.09
^{214}Bi-^{214}Po	0.18 ± 0.10	0.20 ± 0.10
^{13}C(α, n)^{16}O	0.04 ± 0.02	0.04 ± 0.02
Fast neutrons	0.02 ± 0.02	0.02 ± 0.02
Double neutrons	0.05 ± 0.05	0.07 ± 0.05
Atmospheric neutrinos	0.08 ± 0.04	0.07 ± 0.04
Accidentals ($\times 10^{-2}$)	4.9 ± 0.3	4.9 ± 0.3

Table 1 Event selection and backgrounds. The table lists the IBD selection criteria with their respective efficiencies (ε) and relative uncertainties (σ_{rel}), alongside the measured or expected pre-fit and best-fit background rates. The $\bar{\nu}_e$ signal rates were derived both with and without applying the efficiency correction to the observed IBD rate, after background subtraction. The non-oscillated prediction is based on reactor operational data and the flux model described in Methods. The best-fit values for the backgrounds come from the spectral fit.

[1]cpd ≡ counts per day

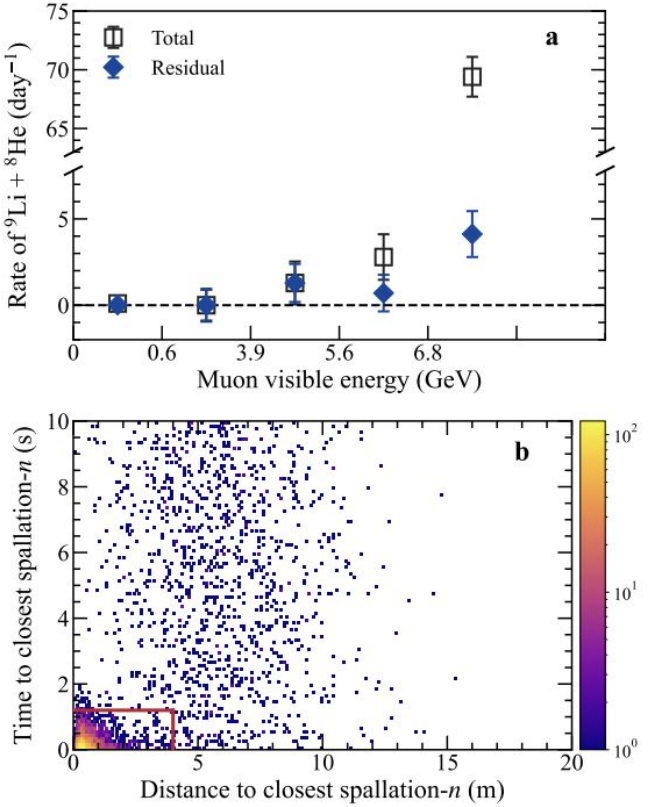

Fig. 9 ^{9}Li/^{8}He background analysis. **a**, Measured ^{9}Li/^{8}He rates across muon visible energy, comparing data before and after the SPN veto. **b**, Spatial- and temporal-distribution of IBD candidates before the SPN cut shown relative to preceding SPN events. A clear cluster of ^{9}Li/^{8}He events is visible at the origin. The red box indicates the SPN veto criteria.

Fermilab

Data Analysis: Reactor-Neutrino Signal Prediction (1)

$$N_i = C \times \int_{E_i^{\mathrm{rec}}}^{E_{i+1}^{\mathrm{rec}}} dE^{\mathrm{rec}} \int dE_{\bar{\nu}_e} \int_{-1}^{1} d\cos\theta \times \sum_r \frac{\mathcal{P}_{ee}(E_{\bar{\nu}_e}, L_r)}{4\pi L_r^2} S_r(E_{\bar{\nu}_e}) \times \frac{d\sigma}{d\cos\theta}(E_{\bar{\nu}_e}, \cos\theta) R(E^{\mathrm{rec}} | E_{\bar{\nu}_e}), \quad (2)$$

IBD cross section

Detector response

Emitted spectrum of core ***r***:

$$S_r(E_{\bar{\nu}_e}) = N_f^r \left[S_{\mathrm{MI}}(E_{\bar{\nu}_e}) + \Delta S_r(E_{\bar{\nu}_e}) \right], \quad (3)$$

calculated using:

- reactor thermal power
- fission fractions
- energy per fission
- spent fuel

Data Analysis: Reactor-Neutrino Signal Prediction (2)

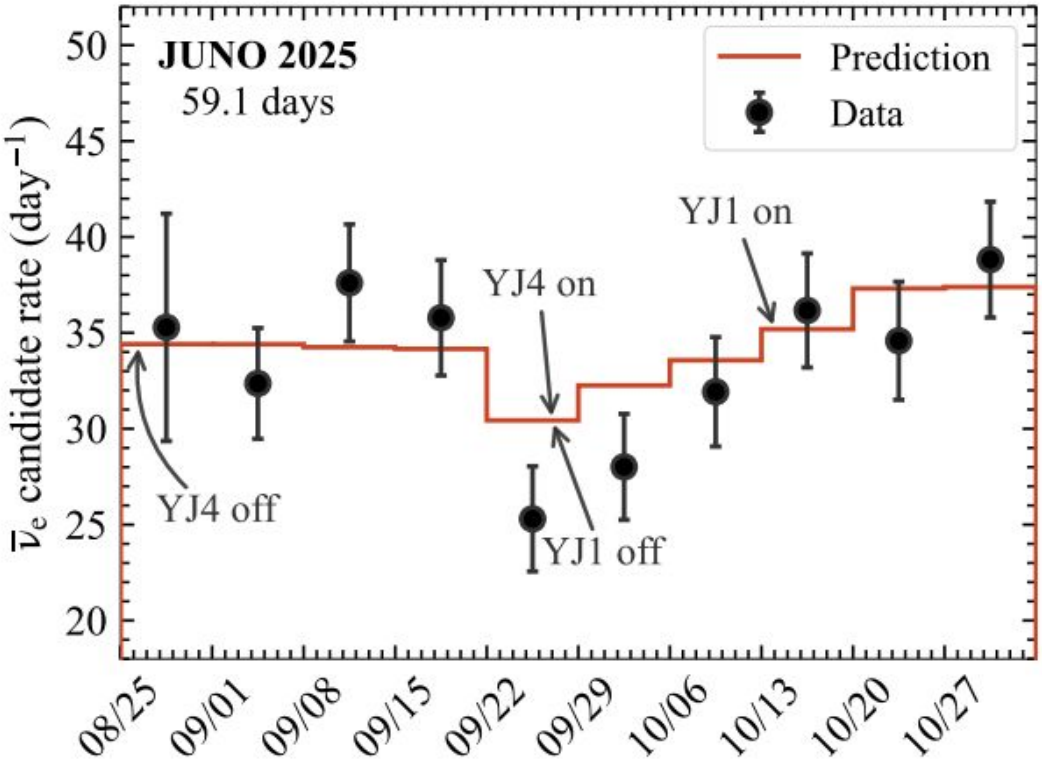

Fig. 10 Temporal distribution of reactor neutrinos. Rates of antineutrino candidates (after subtraction of the mean background rates), shown in one week time bins (black points with statistical error) are compared to the prediction (red line). Arrows indicate operations on the cores YJ1 and YJ4 of the Yangjiang NPP. The NPP reduced the power output due to the occurrence of Super Typhoon Ragasa on September 24th.

Fermilab

Systematic Uncertainties on Prediction

Source	Uncertainties
Target protons	1.0%
Reference spectrum	1.2%
Thermal power	0.5%
Fission fraction	0.6%
Spent nuclear fuel	0.3%
Non-equilibrium	0.2%
Different fission fraction	0.1%

Table 2 Summary of detector and reactor related uncertainties on the predicted reactor neutrino rate.

Spectral Fits

- Distortion primarily shaped by solar oscillation parameters
- □² function for minimization:

$$\chi^2(\vec{p},\eta,\alpha) = (\mu - D)^T V^{-1} (\mu - D) + \lambda^2_{\text{nuis}}(\eta) + \lambda^2_{\text{shape}}(\alpha) + \chi^2_{\text{osc}}(\sin^2\theta_{13}, \Delta m^2_{31}), \quad (5)$$

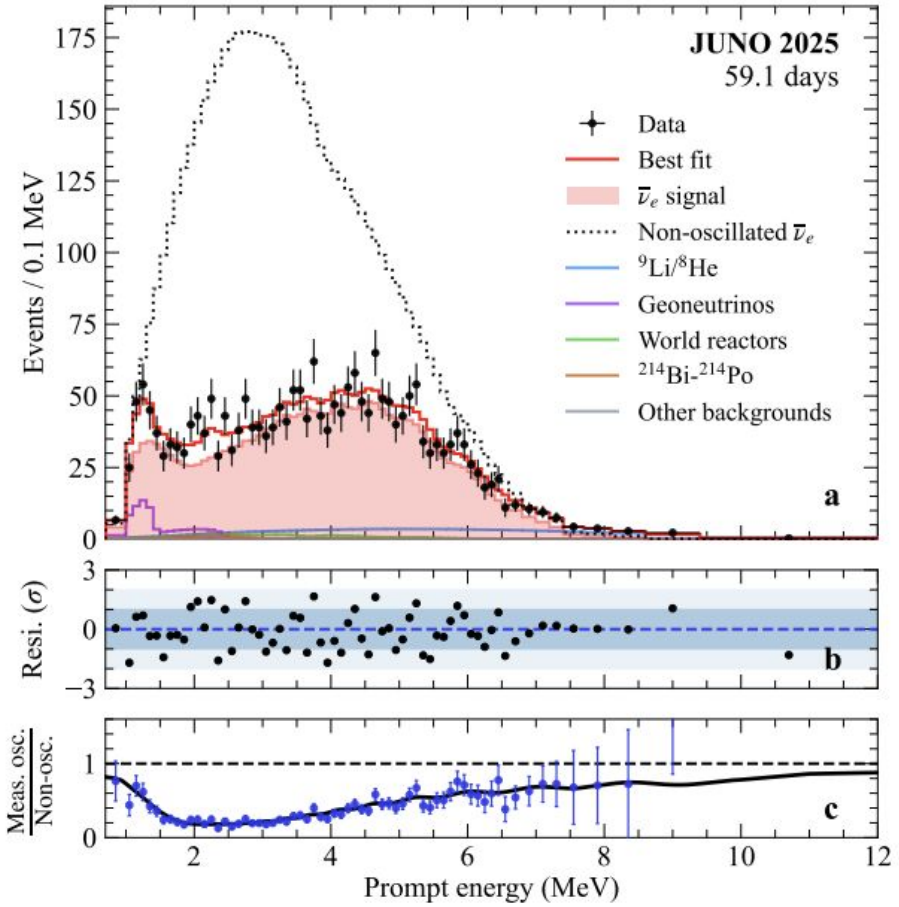

Fig. 3 Measured energy spectrum of prompt IBD candidates. **a**, Black points show measured data with statistical error bars, with the red curve indicating the best-fit oscillation model. Shaded red region represents expected antineutrino signal. Black dotted line represents non-oscillated reactor neutrino expectation. Backgrounds are indicated by other solid color lines. **b**, Residuals quantifying the statistical consistency between data and the complete model. **c**, Ratio of the measured oscillated spectrum to non-oscillated prediction.

Fermilab

Results on Solar Oscillation Parameters

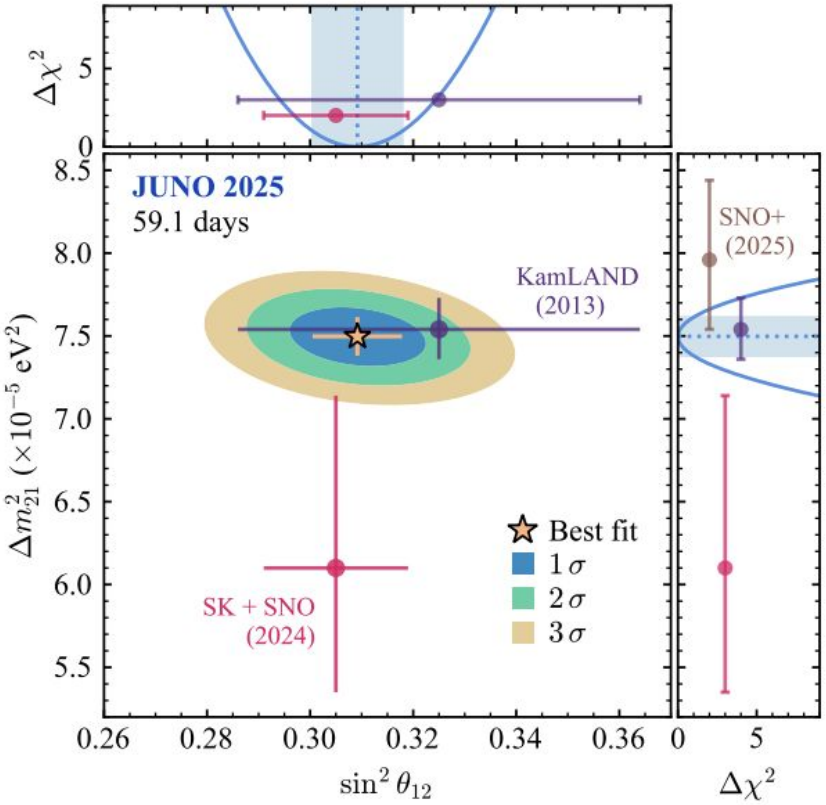

Fig. 4 Results on solar oscillation parameters. Confidence intervals of $\sin^2\theta_{12}$ and Δm^2_{21} from a spectral fit of measured prompt antineutrino energy spectrum shown in Fig. 3. Shaded elliptically-shaped areas correspond to 1σ, 2σ, and 3σ confidence levels. The upper panel provides the one dimensional $\Delta\chi^2$ for $\sin^2\theta_{12}$ obtained by profiling Δm^2_{21} (blue line) and the blue shaded region as the corresponding 1σ interval. The right panel is the same, but for Δm^2_{21}, with $\sin^2\theta_{12}$ profiled. The star marks the best fit values of JUNO, and the error bars show their one-dimensional 1σ confidence intervals. Results from other measurements of reactor neutrinos (KamLAND [13] and SNO+ [54]) and solar neutrinos (combined Super-Kamiokande (SK)+SNO [61]) are shown for comparison.

$$\sin^2\theta_{12} = 0.3092 \pm 0.0087\,,$$
$$\Delta m^2_{21} = (7.50 \pm 0.12) \times 10^{-5}\ \text{eV}^2$$

^ Assumes normal mass ordering
Inverted mass ordering values are comparable

Fermilab

Discussion & Outlook

- Most precise and simultaneous measurement of solar oscillation parameters
  - Improved precision by 1.6x the combination of all previous measurements
- Precision will improve with increased statistics and model-independent analysis using data from JUNO's satellite experiment TAO

Fig. 11 Three analyses post-fit comparison. Post-fit pulls of selected nuisance parameters in the three independent JUNO analysis chains. From left to right, these parameters correspond to the detection efficiency, the double-neutron rate, the ^{9}Li/^{8}He rate, the geoneutrino rate, and the ^{214}Bi-^{214}Po rate. Coloured markers with vertical error bars show the best-fit shift and 1σ uncertainty of each parameter relative to its prior, $(x_{\text{fit}} - x_{\text{prior}})/\sigma_{\text{prior}}$, for Analyses I–III, while the shaded band denotes the $\pm 1\sigma$ prefit range and the dashed line indicates zero pull.

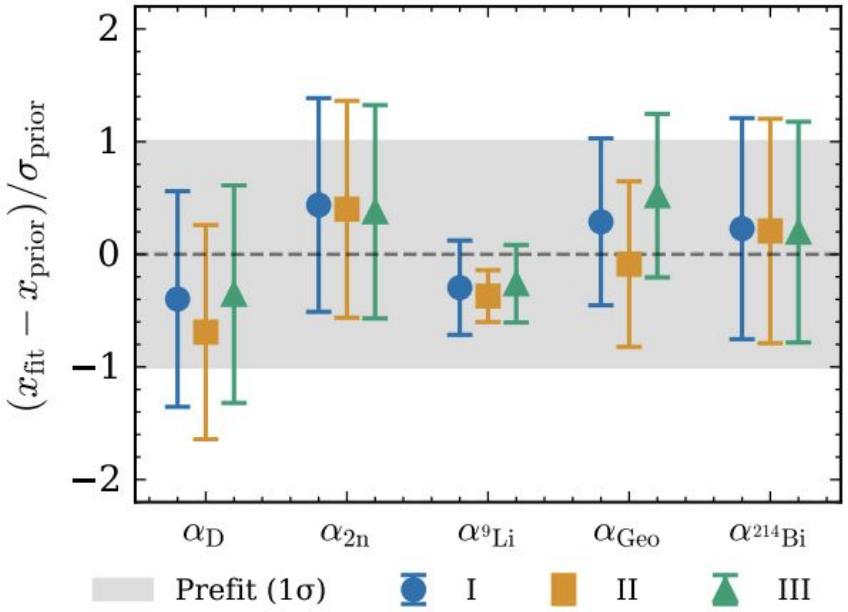

Fermilab